Precision calculation of low-energy electron-impact excitation cross sections of helium among the ground and excited states

De-Ling Zeng,[1,2] Xiang Gao,[2,*] Xiao-Ying Han,[3,†] and Jia-Ming Li[1,4,5]

[1]*Key Laboratory for Laser Plasmas (Ministry of Education) and Department of Physics and Astronomy, Shanghai Jiao Tong University, Shanghai 200240, China*

[2]*Beijing Computational Science Research Center, Beijing 100084, China*

[3]*Institute of Applied Physics and Computational Mathematics, Beijing 100088, China*

[4]*Department of Physics and Center for Atomic and Molecular Nanosciences, Tsinghua University, Beijing, 100084, China*

[5]*Collaborative Innovation Center of Quantum Matter, Beijing 100084, China*

(Received 9 April 2014; revised manuscript received 9 November 2014; published 17 February 2015)

Low-energy electron-impact cross sections of helium among the ground and some low excited states are calculated using the *R*-matrix method. The convergences of the cross sections are checked systematically by using five sets of high-quality target states; i.e., including 5, 11, 19, 29, and 39 physical target states, respectively. Our calculated cross sections are in excellent agreement with the benchmark high-resolution experimental data. Compared with the recommended theoretical data, there is a deviation of about 6%, which suggests the recommended data may need a revision. Based on our calculation results, the influence of the Rydberg target states on the collision cross sections of the excited states is found to be similar to the case of the ground state; i.e., the amplitude of resonance structures will decrease with respect to the principal quantum number n of Rydberg target states. This result should be very useful for providing the cross-section data in the whole energy regions with high quality, which would be of great importance in related scientific fields.

DOI: 10.1103/PhysRevA.91.022707 PACS number(s): 34.80.Dp, 31.15.A−, 31.15.vj

I. INTRODUCTION

The process of electron-impact excitation plays an important role in various fields, such as radiation physics [1], plasma physics [2], atmospheric physics [3], and astrophysics [3–5]. Helium is an abundant element in the universe. Electron-impact excitation cross sections of helium, either from the ground state or from excited states, are indispensable physical parameters for astrophysics [6–10]. Accurate collision cross sections of helium are important in obtaining reliable helium abundances, which can test modern theories of galactic and primordial nucleosynthesis [8].

Helium is probably the simplest and most straightforward atom for the experimental investigation. Detailed experimental studies have been carried out in the past 80 years (see review articles [11–14] and references therein). Although many experimental studies have been carried out, the physical precisions of the scattering cross sections are still difficult to determine. Some experiments are not absolute measurements [15,16]; the normalization strongly depends on the theoretical values. For the absolute measurement experiment, the state-of-the-art experimental precisions are anticipated with only about 10% [17]. For example, absolute measurements of the cross sections (Piech *et al.* [18,19]) often lead to considerable uncertainties, sometimes the uncertainties were even larger than the measured quantities. Therefore, theoretical computations should play an indispensable role to satisfy needs.

With only two electrons, the helium atom is a simple nontrivial many-body system. It provides a perfect testing ground for developing a general method to deal with electron scattering from complex atoms or ions. Over the past decades, a large number of calculations of electron-helium scattering have been performed. For instance, an increasing number of physical targets (5-, 11-, 19-, 29-) states of *R*-matrix calculations of the Belfast group (Berrington *et al.* [20,21], Berrington and Kingston [22], Sawey *et al.* [23]) were carried out. Sawey and Berrington carried out a 29-state *R*-matrix calculation [24] providing total collision strengths for all LS transitions among the lowest 19 ($n \leqslant 4$) states, which are valuable for astrophysics. Fursa and Bray [25] applied the convergent close-coupling (CCC) method to e-He scattering calculation in the incident energy range from 1.5 to 500 eV, where the overall agreement with the experimental data for excitation cross sections from the ground state is good, but without detailed resonance structure. Bartschat [26] carried out an *R*-matrix with pseudostates (RMPS) calculation focusing on the intermediate energy region. Stepanovic *et al.* [16] delivered a joint experimental and theoretical study of near-threshold electron-impact excitation of the $3\,^3S$ and $3\,^1S$ states in helium. With the normalization determined by theoretical work, their joint experimental measurement is in good agreement with their 69-state *B*-spline *R*-matrix (BSR-69) calculation.

However, most works concentrated on the excitation from the ground state; the investigation of excitations from the excited states is limited. Furthermore, distinct discrepancies still exist in different theoretical calculations, especially for the low-energy regions. The dynamical processes in this energy region become very complicated when the resonance structures caused by including higher Rydberg target states are involved. It is difficult to perform calculations at low-energy regions near threshold due to the strong electron correlations. The estimation of the convergence is even more difficult. Earlier, we proposed a calculation scenario to perform the *R*-matrix calculation in low-energy regions in a systematical

*xgao@csrc.ac.cn

†han_xiaoying@iapcm.ac.cn

 ©2015 American Physical Society

way, from which the convergence of the calculation can be examined [27].

In the present work, using the scenario of Ref. [27], we perform an R-matrix calculation of the collision cross sections of helium from ground state $[1s^2]\,1\,^1S$ and the metastable state $[1s2s]\,2\,^3S$ to the $[1s2s]\,2\,^{3,1}S$ and $[1s3s]\,3\,^{3,1}S$ states. The convergence of the calculation is checked systematically through five sets of target states. Meanwhile, the available high-resolution experimental data, i.e., Buckman *et al.* [15] and Stepanovic *et al.* [16], serve as independent benchmarks of our results. Note that these experiments are not absolute measurements and involve the contribution from cascade effects as well. In order to compare with the experiments (1) the experimental data have to be normalized to the precise theoretical calculations. More details will be discussed in Sec. II where we compare our results with the experimental measurements of Buckman *et al.* [15] and Stepanovic *et al.* [16]. (2) Accurate high-excitation scattering cross sections are needed to make cascade corrections. Taking these two facts into account, our calculated cross sections are in excellent agreement with the corresponding experimental measurements. This demonstrates that our high-excitation scattering cross sections are also in good quality, which should be useful for the related applications and will be reported elsewhere. For the excitation processes from the excited states, the absolute measurement data of Piech *et al.* [18,19] provide transitions from the $[1s2s]\,2\,^3S$, but with large uncertainties. As high-resolution measurement of cross sections from lower-excitation states are limited, how to estimate the precision of the calculation from a lower-excitation state is still a difficult problem. In this work, with the cross sections from the ground state accurate enough, we can anticipate the transitions among those states will have the same precision, because we adopt the same sets of convergent target-state wave functions. Compared with the recommended data [24], which are widely used in the astrophysical studies, there is a deviation of about 6%. Such deviation suggests the recommended data should be updated. Furthermore, from our calculation results, the influence of the Rydberg states to the collision cross section from the excited state is elucidated. Amplitude of resonance structures in these cross sections will decrease with respect to the principal quantum number n representing the Rydberg states considered, which is similar to the behavior of the cross section from the ground state [27]. Therefore, it needs only finite physical target states for electron-impact excitation calculations between these lower excited targets. This demonstrates that the cross sections obtained by the partial wave expansion methods valid at low energy could be interfaced with the cross sections obtained by the first Born approximation method valid at high energy [28]. More specifically, the present calculation scenario (including the same target wave functions) can be extended to calculate the partial Born amplitude corrections, which would be very powerful for providing cross-section data with high quality in related scientific fields. We will discuss the calculation of such correction factor in the Conclusions section briefly; more details will be reported elsewhere [29].

II. THEORETICAL METHODS AND CALCULATION RESULTS

Many previous works [20–23,30–35] have given the detailed descriptions of the R-matrix method dealing with the electron-atom collision process. Only a brief description will be presented here. We first briefly describe the approach taken to approximate target wave functions in our calculation, and then describe the scattering calculation. In the present work, based on multiconfiguration self-consistent field (MCSCF) calculation strategies [27,36], we prepare five sets of high-quality target orbital bases using CIVPOL code [37]. These five sets of bases all include pseudo-orbitals, which are used to deal with the important electron correlations. The differences between the five sets of bases are mainly the number of spectroscopy orbitals used to describe the physical target states which correspond to the physical states observed in the spectrum. The orbitals in each set are listed in Table I. The

TABLE I. The basis sets used in the calculations.

Basis set No.	Atomic orbitals (AO)[a]	Physical target states[b]	No. of physical target states
Set 1	$nl(n=1,2\ \ l=0,1)$ $\overline{n}l(\overline{n}=3,4\ \ l=0-3)$	$1s^2\,^1S$, $1s2s\,^{3,1}S$, $1s2p\,^{3,1}P^o$	5
Set 2	$nl(n=1-3\ \ l=0-2)$ $\overline{n}l(n=4,5\ \ l=0-4)$	Set 1[c] + $[1s3s\,^{3,1}S, 1s3p\,^{3,1}P^o, 1s3d\,^{3,1}D]$	11
Set 2′	$nl(n=1-3\ \ l=0-2)$ $\overline{n}l(n=4,5,6\ \ l=0-4)$	Set 1[c] + $[1s3s\,^{3,1}S, 1s3p\,^{3,1}P^o, 1s3d\,^{3,1}D]$	11
Set 3	$nl(n=1-4\ \ l=0-3)$ $\overline{n}l(n=5,6\ \ l=0-4)$	Set 2[c] + $[1s4s\,^{3,1}S, 1s4p\,^{3,1}P^o, 1s4d\,^{3,1}D, 1s4f\,^{3,1}F^o]$	19
Set 4	$nl(n=1-5\ \ l=0-4)$ $\overline{n}l(n=6,7\ \ l=0-4)$	Set 3[c] + $[1s5s\,^{3,1}S, 1s5p\,^{3,1}P^o, 1s5d\,^{3,1}D, 1s5f\,^{3,1}F^o, 1s5g\,^{3,1}G]$	29
Set 5	$nl(n=1-6\ \ l=0-4)$ $\overline{n}l(n=7,8\ \ l=0-4)$	Set 4[c] + $[1s6s\,^{3,1}S, 1s6p\,^{3,1}P^o, 1s6d\,^{3,1}D, 1s6f\,^{3,1}F^o, 1s6g\,^{3,1}G]$	39

[a]One-electron atomic orbitals used to construct the multielectron bases, including the spectroscopy orbitals denoted as nl and polarized pseudo-orbitals denoted as $\overline{n}l$.

[b]Denotes the target states formed by spectroscopy orbitals, represents the physical states observed in the spectrum.

[c]Denotes the physical target states used in the corresponding basis set.

radial parts of these orbitals are expanded in Slater form as

$$P_{nl}(r) = \sum_i c_i r^{p_i} \exp(-\xi i r). \quad (1)$$

More specifically, the five sets of orbital bases are constructed from atomic orbitals including spectroscopy orbitals (labeled as nl and with fixed number of radial nodes, i.e., $n-l-1$) and pseudo-orbitals (labeled as $\bar{n}l$ and without restriction of radial nodes). For $n \leqslant n_p$, where $n_p = 2, \ldots, 6$ for basis sets $p = 1, \ldots, 5$, respectively, the orbitals are optimized as spectroscopy orbitals with the configurations generated by single excitation from $1s^2$ only. In order to consider the electron correlations adequately, we further optimize the $\bar{n} = n_p + 1$ and then $\bar{n} = n_p + 2$ orbitals as pseudo-orbitals with the configurations created by single and double excitations from $1s^2$. In order to check the convergence of the calculations, we further construct Set $2'$ by optimizing the $\bar{n} = n_2 + 3$ pseudo-orbitals to take into account more electron correlations. The spectroscopic orbitals are used to represent the main physical states, while the pseudo-orbitals are used to deal with the important electron correlations, which are specific linear combinations of infinite bound-type Rydberg orbitals and continuum orbitals determined by variational method. Therefore, the pseudostates in our calculation channels have physical meanings, which may be different from the B-spline R-matrix calculations such as Refs. [16,26]. The R-matrix radius, static dipole polarizabilities, and calculated energies for each set are shown in Table II. The pseudo-orbitals are constructed to optimize the energy levels of the physical target states, and the polarizability is not specially optimized, so the polarizability calculated by each set is larger than the experimental value. The calculated energy levels of the corresponding physical target states of the five sets are all in good agreement with the experimental values [38] within 1%, as shown in Table II. Stepanovic *et al.* [16] have a more accurate description of the target wave functions than ours. In order to make a more direct comparison and to confirm the convergence of our calculations, we carry out an extra calculation using Set $2'$. As shown in Table II, the precision of the target states in Set $2'$ is almost at the same level of those in Ref. [16]. By comparing with the cross sections calculated by Set $2'$, we can confirm that the accuracy of our five set calculations is sufficient in the present work. Furthermore, all the calculated thresholds of the five sets were corrected according to the experimental excitation energies. The quantum defects of the target states from our five set calculations are all with good channel properties. More specifically, our calculated quantum defects of different target channels (symmetries) vary slowly with the increase of principal quantum number, and agree excellently with the experimental data. Such agreement means the calculation precisions of various excited target states achieve the same level and demonstrates that the electron correlations of targets are taken into account adequately. Using these sets of "quasicomplete" bases, we can construct configuration interaction (CI) wave functions of the target states with the configurations generated by single and double excitations from $1s^2$. Based on these wave functions, we carefully choose five sets of target terms, respectively, to calculate the collision cross sections. As shown in Table I, Set 1 includes five physical states (with principal quantum number $n \leqslant 2$), Set 2 (and Set $2'$) includes 11 physical states (with $n \leqslant 3$), Set 3 includes 19 physical states (with $n \leqslant 4$), Set 4 includes 29 physical states (with $n \leqslant 5$), while Set 5 includes 39 physical states (with $n \leqslant 6$) to test convergence of other calculations with $n \leqslant 5$, e.g., Sawey and Berrington [24] and Stepanovic *et al.* [16]. By using these sets of target, we can systematically examine the convergence of the scattering calculations and elucidate the influence of the Rydberg states to the collision cross sections.

The total wave function used to describe the collision in the inner region $r < a$, is expanded as

$$\Psi_k(1,2,3) = A \sum_{ij} a_{ijk} \Phi_i(1,2,\hat{r}_3,\sigma_3) u_j(r_3) + \sum_j b_{jk} \phi_j(1,2,3), \quad (2)$$

where the Φ_i are channel functions formed from all the target states in each set, the $u_j(r_3)$ are continuum orbitals that describe the motion of the scattering electron, and the ϕ_j are three-electron bound configurations formed from all the orbitals in each set. The a_{ijk} and b_{jk} coefficients are found by diagonalizing the three-electron Hamiltonian in each basis. For each angular momentum l of the scattering electron, we choose a different number of Lagrange-orthogonalized continuum orbitals for a different set of bases. For example, we choose more than 80 Lagrange-orthogonalized continuum orbitals for Set 5; the highest orbital energies of them are larger than 6.36 Ryd. The total angular momentum of $(N+1)$-electron system is $L = 0-9$. Furthermore, the total wave functions of the three-electron system of the inner region are constructed according to Eq. (2). The bound type three-electron configurations used in the calculations are generated by allowing all the three electrons exciting from the reference configuration $1s^2\,2s^1$. These large number of bound type three-electron configurations are adopted in order to consider the electron correlations within the reaction zone adequately.

Based on the partial cross-section method, we calculated the inelastic scattering cross sections of helium impacted by low-energy electron using the FARM code [39]. Figures 1 and 2 show the convergent properties of the cross section excited from the ground state to the final states of $[1s2s]\,2\,^{3,1}S$, and the comparison with other theoretical results. As the resonance details of the cross sections of Bartschat [26] are not clear, we folded all the theoretical results with 37 meV in Figs. 1(b) and 2(b). The good agreement between Sets 2 and $2'$ demonstrates that the quality of the target-state wave functions in our five sets is good enough for cross-section calculations. The calculated cross sections using the other four target bases sets with more physical target states are consistent with each other except for the five physical target states bases set, which illustrates that five target physical states are not sufficient for the cross-section calculations in this energy region. The differences between the cross sections of the other four target bases sets are only in the energy region above the thresholds of the newly added physical target states, the contributions of which to the cross sections become smaller and smaller and almost negligible at $N > 6$. This result can be understood from the point that when the incident energies increase, more and more channels are opened; hence the contribution of a

TABLE II. Calculated energy levels of the five sets.

		Expt.[a]	Set 1		Set 2		Set2′		Set 3		Set 4		Set 5		Stepanovic *et al.* [16]	
R_0 (a.u.)			19.8		37.2		37.2		55.8		81.2		110.6		90.0	
Polarizability (a.u.)		1.3838	1.566		1.571		1.430		1.564		1.559		1.558			
Absolute energy of ground state (a.u.)		–2.903 724 (Nonrelativistic)	–2.8996		–2.8999		–2.9030		–2.9000		–2.9007		–2.9008		–2.903 479	
Ionization energy (Ryd)		1.807 139	1.7991		1.799 90		1.8061		1.8001		1.8014		1.8016			
Excitation energy (Ryd)	$[1s2s]\,^3S$	1.456 915	1.4495	–0.50%[b]	1.4499	–0.46%[b]	1.4557	–0.08%[b]	1.4501	–0.46%[b]	1.4514	–0.38%[b]	1.4515	–0.37%[b]	1.456 508	–0.03%[b]
	$[1s3s]\,^3S$	1.670 005			1.6628	–0.42%	1.6687	–0.08%	1.6630	–0.41%	1.6643	–0.34%	1.6644	–0.33%	1.669 582	–0.03%
	$[1s4s]\,^3S$	1.734 362							1.7272	–0.40%	1.7286	–0.33%	1.7287	–0.33%	1.733 936	–0.02%
	$[1s5s]\,^3S$	1.762 149									1.7563	–0.33%	1.7564	–0.33%	1.761 722	–0.02%
	$[1s6s]\,^3S$	1.776 632											1.7709	–0.32%		
	$[1s2s]\,^1S$	1.515 439	1.5104	–0.32%	1.5093	–0.39%	1.5146	–0.06%	1.5093	–0.39%	1.5115	–0.26%	1.5115	–0.26%	1.515 160	–0.02%
	$[1s3s]\,^1S$	1.684 843			1.6793	–0.32%	1.6839	–0.06%	1.6786	–0.36%	1.6803	–0.27%	1.6803	–0.27%	1.684 466	–0.02%
	$[1s4s]\,^1S$	1.740 214							1.7343	–0.33%	1.7354	–0.28%	1.7353	–0.28%	1.739 806	–0.02%
	$[1s5s]\,^1S$	1.765 034									1.7604	–0.26%	1.7600	–0.28%	1.764 616	–0.02%
	$[1s6s]\,^1S$	1.778 261											1.7734	–0.27%		
	$[1s2p]\,^3P$	1.541 043	1.5330	–0.51%	1.5338	–0.46%	1.5398	–0.08%	1.5340	–0.45%	1.5354	–0.37%	1.5355	–0.36%	1.540 646	–0.03%
	$[1s3p]\,^3P$	1.691 221			1.6839	–0.42%	1.6900	–0.07%	1.6840	–0.41%	1.6854	–0.35%	1.6855	–0.34%	1.690 802	–0.02%
	$[1s4p]\,^3P$	1.742 737							1.7355	–0.40%	1.7369	–0.34%	1.7370	–0.33%	1.742 312	–0.02%
	$[1s5p]\,^3P$	1.766 284									1.7604	–0.33%	1.7605	–0.33%	1.765 858	–0.02%
	$[1s6p]\,^3P$	1.778 971											1.7732	–0.32%		
	$[1s2p]\,^1P$	1.559 71	1.5523	–0.46%	1.5527	–0.44%	1.5585	–0.08%	1.5528	–0.43%	1.5542	–0.36%	1.5543	–0.35%	1.559 322	–0.02%
	$[1s3p]\,^1P$	1.697 097			1.6900	–0.40%	1.6959	–0.07%	1.6901	–0.40%	1.6915	–0.33%	1.6916	–0.32%	1.696 686	–0.02%
	$[1s4p]\,^1P$	1.745 249							1.7382	–0.39%	1.7395	–0.33%	1.7396	–0.32%	1.744 826	–0.02%
	$[1s5p]\,^1P$	1.767 576									1.7618	–0.33%	1.7619	–0.32%	1.767 150	–0.02%
	$[1s6p]\,^1P$	1.779 72											1.7740	–0.32%		
	$[1s3d]\,^3D$	1.696 115			1.6886	–0.43%	1.6948	–0.08%	1.6888	–0.42%	1.6902	–0.35%	1.6903	–0.34%	1.695 710	–0.02%
	$[1s4d]\,^3D$	1.744 81							1.7375	–0.40%	1.7389	–0.34%	1.7390	–0.33%	1.744 392	–0.02%
	$[1s5d]\,^3D$	1.767 345									1.7614	–0.34%	1.7615	–0.33%	1.766 922	–0.02%
	$[1s6d]\,^3D$	1.779 585											1.7738	–0.33%		
	$[1s3d]\,^1D$	1.696 146			1.6887	–0.43%	1.6948	–0.08%	1.6889	–0.42%	1.6902	–0.35%	1.6903	–0.34%	1.695 740	–0.02%
	$[1s4d]\,^1D$	1.744 828							1.7375	–0.40%	1.7389	–0.34%	1.7390	–0.33%	1.744 410	–0.02%
	$[1s5d]\,^1D$	1.767 356									1.7614	–0.34%	1.7615	–0.33%	1.766 934	–0.02%
	$[1s6d]\,^1D$	1.779 591											1.7738	–0.33%		
	$[1s4f]\,^3F$	1.744 877							1.7376	–0.40%	1.7389	–0.34%	1.7391	–0.33%		
	$[1s5f]\,^3F$	1.767 382									1.7614	–0.34%	1.7616	–0.33%		
	$[1s6f]\,^3F$	1.779 606											1.7738	–0.33%		
	$[1s4f]\,^1F$	1.744 877							1.7376	–0.40%	1.7389	–0.34%	1.7391	–0.33%		
	$[1s5f]\,^1F$	1.767 382									1.7614	–0.34%	1.7616	–0.33%		
	$[1s6f]\,^1F$	1.779 606											1.7738	–0.33%		
	$[1s5g]\,^3G$	1.767 386									1.7614	–0.34%	1.7616	–0.33%		
	$[1s6g]\,^3G$	1.779 609											1.7738	–0.33%		
	$[1s5g]\,^1G$	1.767 386									1.7614	–0.34%	1.7616	–0.33%		
	$[1s6g]\,^1G$	1.779 609											1.7738	–0.33%		

[a]The value of polarizability is taken from [40], accurate nonrelativistic absolute energy of the ground state of He is taken from [41], the ionization energies and excitation energies are taken from [38].

[b]Percentage difference between various calculation results and the experimental data [38], i.e., $(E_{\text{cal.}} - E_{\text{expt.}})/E_{\text{expt.}}$.

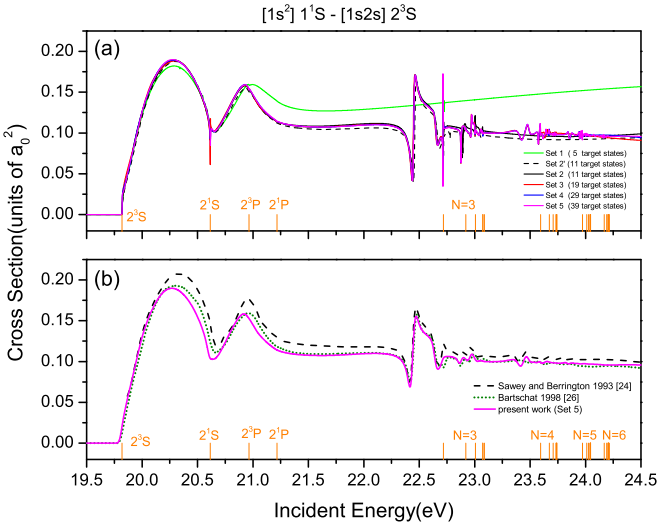

FIG. 1. (Color online) (a) The convergent property of our calculated $[1s^2]\,1\,^1S \rightarrow [1s2s]\,2\,^3S$ cross section. (b) The comparison of our Set 5 calculation with other theoretical results; the cross sections are folded with 37 meV.

specific channel in total resonance structure becomes smaller and smaller. Based on Fig. 1, the uncertainty of our best two bases, i.e., Sets 4 and 5, can be estimated as 0.4% at lower energy around 20.25 eV, and 2.4% at higher energy around 24.25 eV. Based on Fig. 2, the uncertainty can be estimated as 0.9% at lower energy around 21.2 eV, and 2.8% at higher energy around 24.5 eV. It is understandable that the uncertainty at higher energy is greater than that at lower energy, because more target states should be involved at higher energy. At the energy around 22 eV where the cross sections of the two transitions show only a smooth energy dependence, the cross sections of Sawey and Berrington [24] are about 7.8% and 6.8% higher than ours for the $2\,^3S$ and $2\,^1S$ states, respectively;

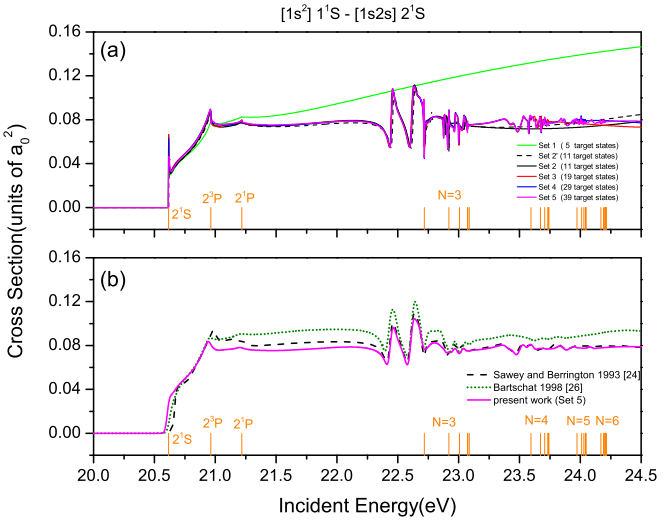

FIG. 2. (Color online) (a) The convergent property of our calculated $[1s^2]\,1\,^1S \rightarrow [1s2s]\,2\,^1S$ cross section. (b) The comparison of our Set 5 calculation with other theoretical results; the cross sections are folded with 37 meV.

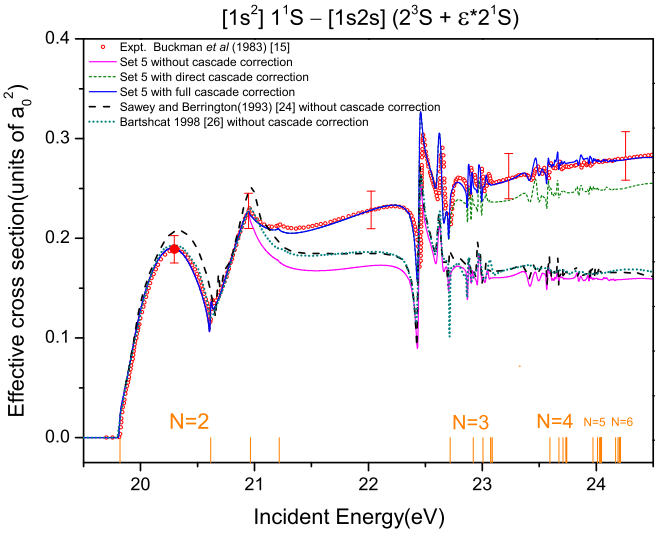

FIG. 3. (Color online) The experimental measurement of the effective cross section of $[1s^2]\,1\,^1S \rightarrow [1s2s]\,(2\,^3S + \varepsilon^* 2\,^1S)$, and the comparison with the theoretical calculations. The experimental measurement is normalized to our theoretical calculation at 20.25 eV (labeled as solid point). According to the experiment, ε is set to be 0.8.

the cross sections of Bartschat [26] are about 1% and 21% higher than ours for the $2\,^3S$ and $2\,^1S$ states, respectively.

Buckman *et al.* [15] measured the yield of metastable atoms resulting from electron-impact excitation of helium. Although the energy resolution is very high, their experiment cannot resolve the two metastable states $2\,^3S$ and $2\,^1S$. Therefore the cross section measured is the effective collision excitation cross section. Figure 5 shows the experimental measurements of the effective collision excitation cross section of helium from the ground state to the two mixed metastable states, and the comparison with our calculated result. According to the detective efficiency of $2\,^3S$ and $2\,^1S$ in the experiment, the weight of the two metastable states in our calculated effective collision excitation cross section is set to 1:0.8 [15]. Since the linewidth of the electron beams used in the experiment is about 5.893 meV [15], in order to compare with the experiment data more clearly, the calculated cross sections are folded with the experimental linewidth. The experimental data of Buckman *et al.* are not absolute measurements, so we have to normalize the experimental data to the theoretical results. In Fig. 3, we normalize the experimental measurements to our calculated cross section at the first peak at 20.25 eV (labeled as solid red circle). In the experiment, any metastable helium atoms ($2\,^1S$ or $2\,^3S$ states) resulting from electron collisions are detected unsolved by a channel electron multiplier. The detected metastable atoms may come from either direct excitation from the ground state, or a cascade of higher excited states. More specifically, when the incident energy is larger than the higher excitation threshold, the higher excited states will also be populated which may cascade down the lower states. Therefore, the cross section measured in the higher-energy region should be taken with the cascade corrections. The population of the metastable state from the cascade process is proportional to the radiative transition rate and the population

of the higher excited state which in turn is proportional to the related impact excitation cross section from the ground state. Hence both the radiative transition rates and the impact excitation cross sections are needed to make the corrections. In our work, the data of radiative transition rates are taken from the NIST values [38]. The related impact excitation cross sections are obtained from our calculations. Using the collision excitation cross sections of our Set 5 calculation, we have made cascade corrections in our calculated cross sections in two cases, i.e., direct cascade correction ($N\,^3P \rightarrow 2\,^3S$, $N\,^1P \rightarrow 2\,^1S$) and full cascade correction (all possible transitions that can cascade to the two metastable states in all possible ways, e.g., $N'\,^3D \rightarrow N\,^3P \rightarrow 2\,^3S$). Compared with experimental results, our calculated cross sections with full cascade correction are in good agreement with experimental data. The uncertainty of the experimental measurement is about 7.5%. The greatest difference between our calculated cross section and the experimental measurement appears at a sharp resonance at about 22.46 eV, where our calculation is 7.6% higher than the experimental measurement. The average difference between our calculation and the experimental measurement is within 1.5%. Sawey and Berrington [24] carried out a 29-state R-matrix calculation, and provide their recommended collision-strength data for all transitions between $N \leqslant 4$ states. We transformed the recommended data from collision strength to cross section, and compare with our calculation and the experiment of Buckman *et al.* Compared with our calculated cross sections without cascade correction, the recommended data are 5.6% higher as a whole. At the peak of the cross section, where there is no cascade contribution, the recommended data are 9.8% higher than the experiment. In the energy region of 21.4–22.1 eV, where the cross section shows only a smooth energy dependence, the cross section of Sawey and Berrington [24] is about 8.5% higher than ours. We also made a comparison with Bartschat [26], the effective cross section of which is 4.6% higher than ours as a whole. The calculation of Bartschat agrees well with our result and the experiment in the energy region below 21 eV. But for the energy region between 21.4 and 22.1, where the cross section shows only a smooth energy dependence, the result of Bartschat is 7.9% higher than our result without cascade correction.

Figures 4 and 5 show the convergent properties of the cross section excited from the ground state to the final states of $[1s3s]\,3\,^{3,1}S$, and the comparison with other theoretical results. As the resonance details of the cross sections of Bartschat [26] are not clear, we folded all the theoretical results with 37 meV in Figs. 3(b) and 4(b). The convergence of the two excitation cross sections behaviors is similar to that of $[1s^2]\,1\,^1S \rightarrow [1s2s]\,2\,^{3,1}S$ cross sections. Based on Fig. 4, the uncertainty of our best two bases, i.e., Sets 4 and 5, can be estimated as 2.4% at lower energy around 22.8 eV, and 7.8% at higher energy around 24.3 eV. Based on Fig. 5, the uncertainty can be estimated as 8.6% at lower energy around 22.94 eV, and 12.7% at higher energy around 24.3 eV. At the energy around 23.2 eV where the cross sections of the two transitions show only a smooth energy dependence, the results of Sawey and Berrington [24], Bartschat [26], and Stepanovic *et al.* [16] are about 9.2%, 10.3%, and 6.5% higher than ours for the $3\,^3S$ state, while for the $3\,^1S$ state, they are 12.7%, 12.7%, and

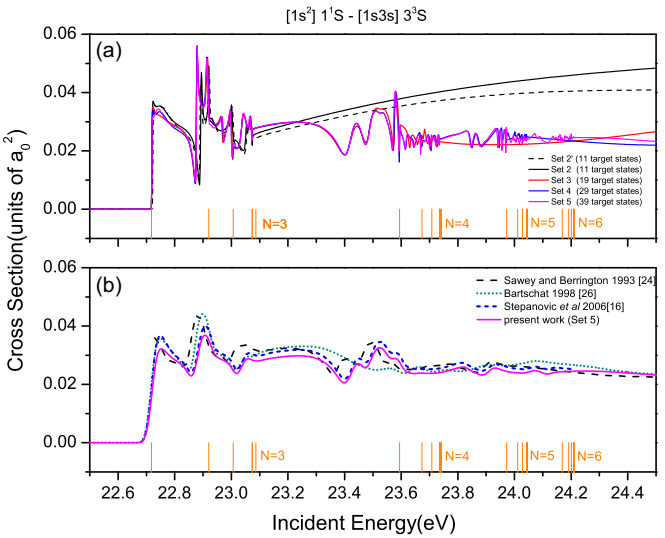

FIG. 4. (Color online) (a) The convergent property of our calculated $[1s^2]\,1\,^1S \rightarrow [1s3s]\,3\,^3S$ cross section. (b) The comparison of our Set 5 calculation with other theoretical results; all the results were folded with 37 meV.

21.5% higher, respectively. For other cross sections excited from the ground state, the convergence behaviors are similar.

Figures 6 and 7 show the comparison of theoretical calculations with the precise experimental measurements for the collision excitation cross section of helium from ground state to the final states of $[1s3s]\,3\,^3S$ and $3\,^1S$ states, respectively. All the calculated cross sections are folded with 37 meV as the experimental linewidth. Since the cross sections of the two transitions are not absolute measurements, the experimental measurements are normalized to the BSR-69 calculations at the point of 23.2 eV [16] (labeled as solid diamond) in order to compare with the theoretical results, as shown in Figs. 6(a)

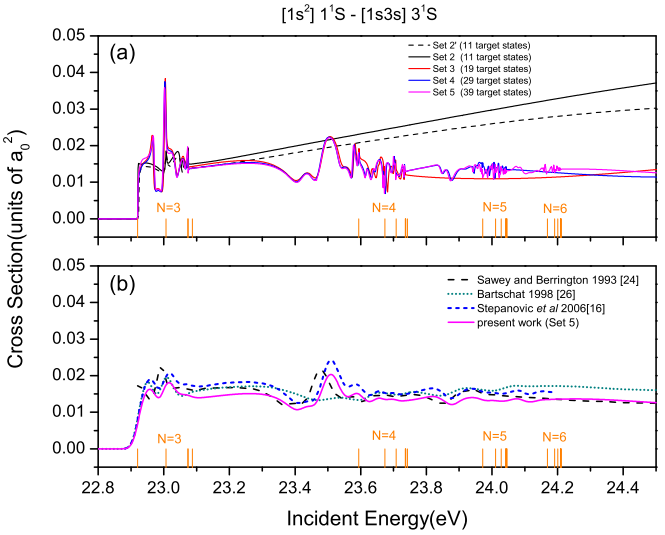

FIG. 5. (Color online) (a) The convergent property of our calculated $[1s^2]\,1\,^1S \rightarrow [1s3s]\,3\,^1S$ cross section. (b) The comparison of our Set 5 calculation with other theoretical results; all the results were folded with 37 meV.

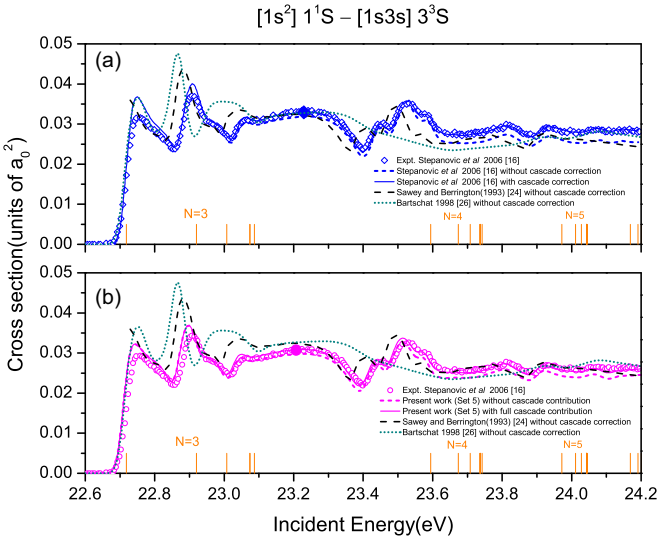

FIG. 6. (Color online) The experimental measurement of the excitation cross section of $[1s^2]\,1\,{}^1S \rightarrow [1s3s]\,3\,{}^3S$, and comparison with the theoretical calculations. The experimental measurements are normalized to the theoretical ones at 23.2 eV (labeled as solid point), respectively.

and 7(a). We do the same normalization of the experiment to our calculation at the same point of 23.2 eV (labeled as solid circle) in Figs. 6(b) and 7(b). The cascade contribution was found to be important for the $3\,{}^3S$ excitation, whereas it is negligible (less than 1%) for the $3\,{}^1S$ state [16]. Both the BSR-69 calculation and ours have taken into account the cascade corrections for the ${}^3S$ state. The theoretical results of Sawey and Berrington [24] and Bartschat [26] are without cascade correction for both the two states.

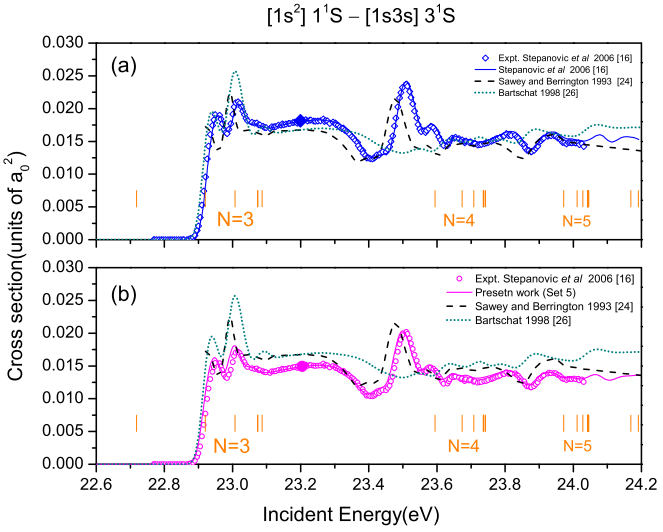

FIG. 7. (Color online) The experimental measurement of the excitation cross section of $[1s^2]\,1\,{}^1S \rightarrow [1s3s]\,3\,{}^1S$, and comparison with the theoretical calculations. The experimental measurements are normalized to the theoretical ones at 23.2 eV (labeled as solid point), respectively.

As for the $[1s3s]\,3\,{}^3S$ excitation cross section shown in Fig. 6, both the BSR-69 calculation and ours with cascade contribution are in good agreement with the normalized experimental measurements, except for the first two resonance structures, where the theoretical results are somewhat higher than the experimental measurements. For the first resonance structure, the BSR-69 result is 16.3% higher than the experimental data while our result is 10.1% higher; for the second resonance structure, the BSR-69 result is 8.3% higher than the experimental data while our result is 7.4% higher. The ratio between the first two resonance structures is 0.85 for experimental measurements, 0.92 for the BSR-69 calculation, and 0.87 for our Set 5 calculation. More computation efforts and further experimental measurement are needed to investigate this deviation. Although both the BSR-69 calculation and ours are in good agreement with the normalized experimental measurements, the BSR-69 calculation is about 10% higher than our calculated cross section as a whole. The resonant profiles of Sawey and Berrington [24] and Bartschat [26] do not show a good agreement with the experiment. The 46-state RMPS calculations of Bartschat show only resonances below the $N = 3$ threshold, because they only include physical states of $N = 1-3$. Compared with our result at the energy around 23.2 eV where there is no cascade contribution and the cross section shows only a smooth energy dependence, the result of Sawey and Berrington [24] is about 9.2% higher, while Bartschat [26] and the BSR-69 calculation is about 10.3% and 6.5% higher than our result, respectively. The recommended data of Sawey and Berrington [24] is 5% higher than ours as a whole.

As for the $[1s3s]\,3\,{}^1S$ excitation cross section shown in Fig. 7, both the results of BSR-69 and ours are in excellent agreement with the normalized experimental measurements. The BSR-69 calculation is about 15% higher than our calculated cross section as a whole. The resonant profiles of Sawey and Berrington [24] and Bartschat [26] do not show a good agreement with the experiment. Compared with our result, both the cross sections of Sawey and Berrington [24] and Bartschat [26] are 12.7% higher than ours at 23.2 eV, while the BSR-69 calculation is 21.5% higher. The recommended data of Sawey and Berrington [24] are 7.8% higher than ours as a whole. From Figs. 6 and 7 we can note that the normalization of experimental measurement to the theoretical calculations may not be enough; absolute measurement is important.

Using the same basis sets, we calculated the cross sections from excited states of helium. Figures 8 and 9 show our calculated collision excitation cross section of helium from $[1s2s]\,2\,{}^3S$ to the final states of $[1s3s]\,3\,{}^3S$ and $3\,{}^1S$ respectively, and the comparison with other theoretical calculations and experimental measurements. The available experimental measurements shown in Fig. 8 are from Piech *et al.* [18,19]. We have subtracted the cascade contribution from the experimental measurements using our calculated high-excitation cross sections. Since the high-precision experimental data and theoretical data are relatively rare for these excitation cross sections, in order to verify the precision of our calculated cross sections from excited states, we note that there exist cross sections excited from the ground state, which can be accurately measured by experiment as discussed above. Considering the R-matrix method treats the excitation from

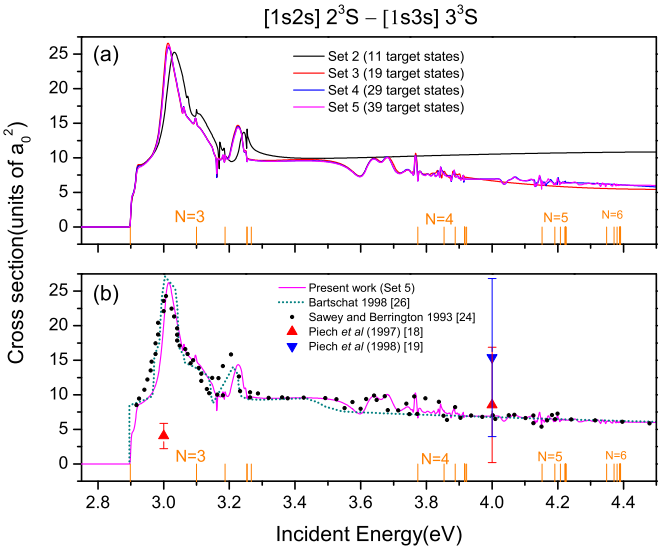

FIG. 8. (Color online) (a) The convergent property of our calculated $[1s2s]\,2\,^3S \rightarrow [1s3s]\,3\,^3S$ cross section. (b) The comparison of our Set 5 calculation with other theoretical results and experiments.

the ground state and from lower excited states on equal footing; the good calculated cross sections from the ground state indicate high-quality wave functions of the final states of these excitations. Then the precision of the cross sections between these excited states can be guaranteed. Therefore, our calculated collision excitation cross sections of helium from ground state to the states of $2\,^{3,1}S$ and $3\,^{3,1}S$, which have been accurately measured by experiments, can be used as a precise criterion for evaluating the accuracy of the cross sections $2\,^3S \rightarrow 3\,^{3,1}S$. As shown in Figs. 8 and 9, our calculated cross sections using the four sets of 11, 19, 29, and 39 physical target states are consistent with each other, which demonstrate the good quality of our calculations. The

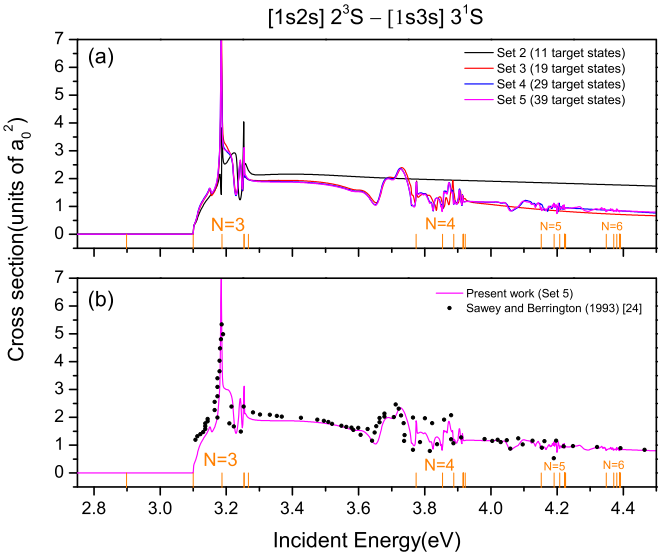

FIG. 9. (Color online) (a) The convergent properties of our calculated $[1s2s]\,2\,^3S \rightarrow [1s3s]\,3\,^1S$ cross section. (b) The comparison of our Set 5 calculation with other theoretical result.

differences between the four target bases sets are only in the energy region above the thresholds of the newly added physical target states, the contributions of which to the cross sections become smaller and smaller and almost negligible at $N > 6$. Based on Fig. 8(a), the uncertainty of our best two bases, i.e., Sets 4 and 5, can be estimated as 0.1% at lower energy around 3.02 eV, and 3.4% at higher energy around 4.5 eV. Based on Fig. 9(a), the uncertainty of our best two bases, i.e., Sets 4 and 5, can be estimated as 2.0% at lower energy around 3.20 eV, and 4.1% at higher energy around 4.5 eV. It is also understandable that the uncertainty at higher energy is greater than that at lower energy, because more target states will be involved in at higher energy. The 46-state RMPS calculation of Bartschat [26] shows only resonance structures near the $N = 3$ threshold, because they only include physical $N = 1$–3 states. The results of Sawey and Berrington [24] agree well with our calculations for both the two cross sections as a whole (4.3% higher for the $[1s2s]\,2\,^3S \rightarrow [1s3s]\,3\,^3S$ cross section and 8.4% higher for the $[1s2s]\,2\,^3S \rightarrow [1s3s]\,3\,^1S$ cross section). But in some strongly resonant regions, there exist considerable deviations between the result of Sawey and Berrington [24] and our calculation. For instance, in around 3.8 eV, their result is 27.7% larger than ours for the $[1s2s]\,2\,^3S \rightarrow [1s3s]\,3\,^3S$ transition cross section, and 59.6% larger than ours for the $[1s2s]\,2\,^3S \rightarrow [1s3s]\,3\,^1S$ transition cross section. More work will be done to present cross sections from metastable states to higher excited states, and compared with the available experiments.

III. CONCLUSIONS

Finally, we would like to conclude by the following remarks. In the present work, we have systematically checked the convergence property of all our calculations via five sets of target state wave functions in theory, and compared with experimental measurements for the effective collision cross section of $[1s^2]\,1\,^1S \rightarrow [1s2s]\,(2\,^3S + \varepsilon^* 2\,^1S)$ and the cross sections of $[1s^2]\,1\,^1S \rightarrow [1s3s]\,3\,^3S$ and $[1s^2]\,1\,^1S \rightarrow [1s3s]\,3\,^1S$ to further examine the convergence of our calculations. The most common method to measure cross sections in experiments is to obtain the fluorescence signal of the excited states, so the cross section measured in a higher-energy region will be mixed with cascade contributions. Our theoretical results of $[1s^2]\,1\,^1S \rightarrow [1s2s]\,(2\,^3S + \varepsilon^* 2\,^1S)$ and $[1s^2]\,^1S \rightarrow [1s3s]\,3\,^{3,1}S$ cross sections, in which cascade corrections are considered adequately, are in excellent agreement with the experimental measurements. Such agreement demonstrates that our calculated high-excitation cross sections should be accurate enough. As space is limited, our other cross sections will be presented in another paper in a form that is convenient for the readers. As high-resolution measurements of cross sections from lower excitation states are limited, how to estimate the precision of the calculation from a lower excitation state is still a difficult problem. In this work, our calculated cross sections of $[1s^2]\,1\,^1S \rightarrow [1s2s]\,(2\,^3S + \varepsilon^* 2\,^1S)$ and $[1s^2]\,^1S \rightarrow [1s3s]\,3\,^{3,1}S$ have been accurately examined by benchmark experiments; we can guarantee the transitions among those excitation states will have the same precision. Compared with our results, the recommended data [24] are 5.6% higher for the $[1s^2]\,1\,^1S \rightarrow [1s2s]\,(2\,^3S + \varepsilon^* 2\,^1S)$ cross section, 5.0% higher

for the $[1s^2]\,^1S \rightarrow [1s3s]\,3\,^3S$ cross section, 7.8% higher for the $[1s^2]\,1\,^1S \rightarrow [1s3s]\,3\,^1S$ cross section, 4.3% higher for the $[1s2s]\,2\,^3S \rightarrow [1s3s]\,3\,^3S$ cross section, and 8.4% higher for the $[1s2s]\,2\,^3S \rightarrow [1s3s]\,3\,^1S$ cross section. Such deviation suggests the recommended data should be updated.

High-resolution experiments are mostly not absolute measurements [15,16]; the normalization strongly depends on the theoretical values. There are still some problems in the normalization to the theoretical values. As for the examples of $[1s^2]\,1\,^1S \rightarrow [1s3s]\,3\,^{3,1}S$ cross sections, both the BSR-69 [16] and our Set 5 calculations are in excellent agreement with the normalized measurements, while our Set 5 calculation is 15% lower than the BSR-69 calculation [16] for the $[1s^2]\,^1S \rightarrow [1s3s]\,3\,^1S$ cross section, and 10% lower than the BSR-69 calculation [16] for the $[1s^2]\,1\,^1S \rightarrow [1s3s]\,3\,^3S$ cross section. Moreover, for the first two resonance structures near threshold of the $[1s^2]\,^1S \rightarrow [1s3s]\,3\,^3S$ cross section, the ratio between them is 0.85 for experimental measurements, 0.92 for the BSR-69 calculation [16], and 0.87 for our Set 5 calculation closer to the experimental value. Note that the normalization of experimental measurements to the theoretical calculations may not be enough; absolute measurement is important, so we appeal for further study of absolute measurement, even for simple systems like helium.

The influence of Rydberg states has been shown in Figs. 1, 2, 4(a), 5(a), 8(a), and 9(a), where the amplitudes of resonance structures decrease with the increasing principal quantum number n, which represents the Rydberg states involved. This means that contributions of the resonance structure to these collision cross sections are not important at higher incident energies. Therefore, we need only finite physical target states to perform calculations. This result also demonstrates that the cross sections obtained by the partial wave expansion methods valid at low energy could be interfaced with the cross sections obtained by the first Born approximation method valid at high energy [27]. More specifically, starting from Born approximations [28], the scattering amplitude f can be calculated by $f = f^{Born} + \Delta f$, where the correction function Δf can be calculated by partial wave expansions involving only a finite number of penetrating partial waves (low angular momentums), which would be very powerful for providing cross-section data in intermediate-energy regions with high quality for related scientific fields. Our work on how to efficiently interface the cross sections of low incident energies and high incident energies is in progress and will be reported elsewhere [29].

ACKNOWLEDGMENTS

This work is supported by the National Science Foundation of China (Grants No. 11274035, No. 11328401, No. 11474031, No. 11371218, and No. 11275029), the National Basic Research Program (Grants No. 2010CB922900, No. 2011CB921501, and No. 2013CB922200), Ministry of Science and Technology and Ministry of Education of China, the Key grant project of Chinese Ministry of Education (Grant No. 306020), National High-Tech ICF committee of China, and the Yin-He Super-computer Center.

[1] L. G. Christophorou, *Atomic and Molecular Radiation Physics* (John Wiley & Sons Ltd, New York, 1971).
[2] J. D. Lindl, P. Amendt, R. L. Berger, S. G. Glendinning, S. H. Glenzer, S. W. Haan, R. L. Kauffman, O. L. Landen, and L. J. Suter, Phys. Plasmas **11**, 339 (2004).
[3] A. Dalgarno, Adv. At. Mol. Phys. **15**, 37 (1979).
[4] T. R. Kallman and P. Palmeri, Rev. Mod. Phys. **79**, 79 (2007).
[5] P. Beiersdorfer, Annu. Rev. Astron. Astrophys. **41**, 343 (2003).
[6] D. P. Smits, Mon. Not. R. Astron. Soc. **278**, 683 (1996).
[7] R. A. Benjamin, E. D. Skillman, and D. P. Smits, Astrophys. J. **514**, 307 (1999).
[8] J. Kingdon and G. J. Ferland, Astrophys. J. **442**, 714 (1995).
[9] H. -J. Kunze and W. D. Johnston III, Phys. Rev. A **3**, 1384 (1971).
[10] I. Bray, A. Burgess, D. V. Fursa, and J. A. Tully, Astron. Astrophys. Suppl. Ser. **146**, 481 (2000).
[11] B. Bederson and L. J. Kieffer, Rev. Mod. Phys. **43** 601 (1971).
[12] D. W. O. Heddle and J. W. Gallagher, Rev. Mod. Phys. **61** 221 (1989).
[13] C. C. Lin and L. W. Anderson, Adv. At. Mol. Phys. **29**, 1 (1992).
[14] S. Nakazaki, Adv. At. Mol. Phys. **30**, 1 (1993).
[15] S. J. Buckman, P. Hammond, F. H. Read, and G. C. King, J. Phys. B: At. Mol. Phys. **16**, 4039 (1983); J. N. H. Brunt, G. C. King, and F. H. Read, *ibid.* **10**, 433 (1977).
[16] M. Stepanovic, M. Minic, D. Cvejanovic, J. Jureta, J. Kurepa, S. Cvejanovic, O. Zatsarinny, and K. Bartschat, J. Phys. B: At. Mol. Phys. **39**, 1547 (2006).
[17] C. C. Lin and J. B. Boffard, Adv. At. Mol. Phys. **51**, 385 (2005).
[18] G. A. Piech, M. E. Lagus, L. W. Anderson, C. C. Lin, and M. R. Flannery, Phys. Rev. A **55**, 2842 (1997).
[19] G. A. Piech, J. E. Chilton, L. W. Anderson, and C. C. Lin, J. Phys. B: At. Mol. Phys. **31**, 859 (1998).
[20] K. A. Berrington, P. G. Burke, and A. L. Sinfailam, J. Phys. B: At. Mol. Phys. **8**, 1459 (1975).
[21] K. A. Berrington, P. G. Burke, L. C. G. Freitas, and A. E. Kingston, J. Phys. B: At. Mol. Phys. **18**, 4135 (1985).
[22] K. A. Berrington and A. E. Kingston, J. Phys. B: At. Mol. Phys. **20**, 6631 (1987).
[23] P. M. J. Sawey, K. A. Berrington, P. G. Burke, and A. E. Kingston, J. Phys. B: At. Mol. Phys. **23**, 4321 (1990).
[24] P. M. J. Sawey and K. A. Berrington, At. Data Nucl. Data Tables **55**, 81 (1993).
[25] D. V. Fursa and I. Bray, Phys. Rev. A **52**, 1279 (1995).
[26] K. Bartschat, J. Phys. B: At. Mol. Phys. **31**, L469 (1998).
[27] X. Gao, X. Y. Han, L. Voky, N. Feautrier, and J. M. Li, Phys. Rev. A **81**, 022703 (2010).
[28] X. Y. Han and J. M. Li, Phys. Rev. A **74**, 062711 (2006); X. Y. Han, Y. M. Li, H. Zhang, J. Yan, J. M. Li, and L. Voky, *ibid.* **78**, 052702 (2008).
[29] X. Y. Han, X. Gao, D. L. Zeng, and J. M. Li (unpublished).
[30] P. G. Burke, A. Hibbert, and W. D. Robb, J. Phys. B **4**, 153 (1971).
[31] K. A. Berrington, P. G. Burke, J. J. Chang, A. T. Chivers, W. D. Robb, and K. T. Taylor, Comput. Phys. Commun. **8**, 149 (1974).

[32] K. A. Berrington, P. G. Burke, M. Le Dourneuf, W. D. Robb, K. T. Taylor, and L. VoKy, Comput. Phys. Commun. **14**, 367 (1978).
[33] K. A. Berrington, P. G. Burke, K. Butler, M. J. Seaton, P. J. Storey, K. T. Taylor, and Y. Yan, J. Phys. B **20**, 6379 (1987).
[34] L. VoKy, H. E. Saraph, W. Eissner, Z. W. Liu, and H. P. Kelly, Phys. Rev. A **46**, 3945 (1992).
[35] K. A. Berrington, W. B. Eissner, and P. H. Norrington, Comput. Phys. Commun. **92**, 290 (1995).
[36] B. Qing, C. Cheng, X. Gao, X. L. Zhang, and J. M. Li, Acta Phys. Sin. **59**, 145 (2010) (in Chinese).
[37] A. Hibbert, Comput. Phys. Commun. **9**, 141 (1975).
[38] Y. Ralchenko, A. E. Kramida, J. Reader, and NIST ASD Team (2008). NIST Atomic Spectra Database (version 3.1.5) online. Available at http://physics.nist.gov/PhysRefData/ASD/levels_form.html (January 7, 2010) (National Institute of Standards and Technology, Gaithersburg, MD, 2008).
[39] V. M. Burke and C. J. Noble, Comput. Phys. Commun. **85**, 471 (1995).
[40] P. W. Langhoff and M. Karplus, J. Opt. Soc. Am. **59**, 863 (1969).
[41] C. L. Pekeris, Phys. Rev. **112**, 1649 (1958).